

Oil-lubricated sliding wear performance of TiSiCN-coated ductile iron

Forest C. Thompson^a, Frank M. Kustas^b, Grant A. Crawford^{a,*}

^a Arbegast Materials Processing & Joining Laboratory, South Dakota School of Mines and Technology, Rapid City, USA

^b NanoCoatings, Inc., Rapid City, USA

ARTICLE INFO

Keywords:

Internal combustion engines
Lubricated wear
Cast iron
PVD coatings

ABSTRACT

Improvements to internal combustion engine performance can be achieved by the application of advanced coatings to piston rings and cylinder bores. Here, the sliding wear performance of TiSiCN coatings on ductile iron was evaluated in heavy-duty diesel engine oil using a block-on-ring tribometer. The coatings were deposited by plasma-enhanced magnetron sputtering of titanium in a reactive environment containing nitrogen, acetylene, and hexamethyldisilazane. Coating characterization was conducted using X-ray spectroscopy and diffraction, electron microscopy, and nanoindentation. TiSiCN adhesion to ductile iron was qualified by Rockwell indentation testing. Wearing surface and counter surface material pairs were systematically varied. Intermittent friction oscillation was observed for self-mated TiSiCN, while tribosystems with only one TiSiCN surface exhibited improved friction stability relative to uncoated ductile iron. A 24% reduction in block wear rate was achieved by coating the block surface with TiSiCN. Solely coating ring surfaces with TiSiCN, however, increased the uncoated block wear rate by over 300%.

1. Introduction

Ductile iron (also known as spheroidal-graphite cast iron) finds use in components requiring relatively high strength and toughness including gears, crankshafts, engine blocks, and piston rings [1,2]. While certain grades of ductile iron, such as grade 100-70-03 (UNS F34800), provide excellent combinations of strength, wear resistance, and low coefficients of friction [2], enhanced tribological performance of ductile iron is required for certain applications. Specifically, friction and wear of power cylinder components in heavy-duty engines (e.g., piston rings, cylinder liners) must be better controlled to improve fuel economy, decrease engine oil consumption, and reduce maintenance costs [3]. This can be achieved through mechanical design, lubricant technologies, and/or surface engineering [3].

Protective coatings produced by physical vapor deposition (PVD) techniques are well-suited to meet the surface engineering requirements of many internal combustion engine components. Nanostructured PVD coatings based on transition metal nitrides or carbides (e.g., TiN, CrN, TiC) demonstrate exceptional tribological performance due to the ability to tailor their hardness [4], thermal stability [5], toughness [6,7], and friction coefficients [8] for specific operating environments. Mature PVD techniques are available for the deposition of these ceramic

materials onto the cylinder bore and the outer surface of piston rings [9, 10]. Unlike thick coatings, such as those produced by thermal spray or laser cladding technologies, thin PVD coatings inherit the surface topography of the component substrate, which is critical for the performance of cylinder liners with surface finishes honed for optimum lubricant retention [11]. Additionally, PVD processes are safe alternatives to chrome plating, which has traditionally been used to modify the surface of both ductile iron piston rings and cylinder liners [2,12]. The durability and long-term reliability of components coated by PVD is ensured by achieving excellent adhesion through *in situ* plasma cleaning of substrate surfaces prior to deposition [13] and by utilizing various process levers to tailor residual stress profiles for the expected service conditions [14].

Recently, low friction TiSiCN nanocomposite coatings have been shown to be an attractive material system for piston ring applications [15]. When deposited by an advanced PVD technique called plasma-enhanced magnetron sputtering (PEMS) [16], the TiSiCN microstructure consists of a nanocrystalline TiC_xN_y phase embedded in an intergranular, amorphous SiC_xN_y phase [17]. The nanocomposite architecture imparts excellent toughness to the coating while maintaining high hardness, ultimately resulting in excellent sliding wear and erosion resistance [18,19]. To achieve a low coefficient of friction

* Corresponding author. Arbegast Materials Processing & Joining Laboratory, South Dakota School of Mines and Technology, 501 E. Saint Joseph Street, Rapid City, SD, 57701, USA.

E-mail address: Grant.Crawford@sdsmt.edu (G.A. Crawford).

Table 1

TiSiCN source material deposition conditions and layer growth durations.

Coating	Ti	N ₂	C ₂ H ₂	HMDS	Interlayer	Top Layer
	Power (W)	Flow Rate (SCCM)	Flow Rate (SCCM)	Flow (divisions)	Duration (min)	Duration (min)
TiSiCN-L	1000	23.3	10.4	20	77.0	101.5
TiSiCN-H	1000	23.3	10.4	25	77.0	127.1
TiSiCN-L-BLOCKS	1000	23.3	10.4	20	77.0	105.7
TiSiCN-L-RINGS	1000	23.3	10.4	20	95.4	166.4

Table 2

Block-on-ring sliding wear test plan.

Test #	Block	Block	Ring	Ring	Oil Type/Temperature	Normal Load (N)	Sliding Speed (m/s)	Sliding Distance (m)
	Coating	Material	Coating	Material				
1	Uncoated	Ductile Iron	Uncoated	Falex S-10	15W-40	222	0.2	200
		100-70-03		SAE 4620	127°C			
2	TiSiCN-L	Falex H-30	Uncoated	Falex S-10	15W-40	222	0.2	200
		SAE O1		SAE 4620	127°C			
3	TiSiCN-H	Falex H-30	Uncoated	Falex S-10	15W-40	222	0.2	200
		SAE O1		SAE 4620	127°C			
4–5	Uncoated	Ductile Iron	Uncoated	Falex S-10	15W-40	222	0.2	200
		100-70-03		SAE 4620	127°C			
6–8	TiSiCN-L-BLOCKS	Ductile Iron	Uncoated	Falex S-10	15W-40	222	0.2	200
		100-70-03		SAE 4620	127°C			
9–11	Uncoated	Ductile Iron	TiSiCN-L-RINGS	Falex S-10	15W-40	222	0.2	200
		100-70-03		SAE 4620	127°C			
12–14	TiSiCN-L-BLOCKS	Ductile Iron	TiSiCN-L-RINGS	Falex S-10	15W-40	222	0.2	200
		100-70-03		SAE 4620	127°C			

Table 3

Elemental compositions of the developmental TiSiCN coatings.

Coating	Ti (at.%)	Si (at.%)	C (at.%)	N (at.%)	O (at.%)
TiSiCN-L	28	3	34	33	2
TiSiCN-H	25	5	37	32	1

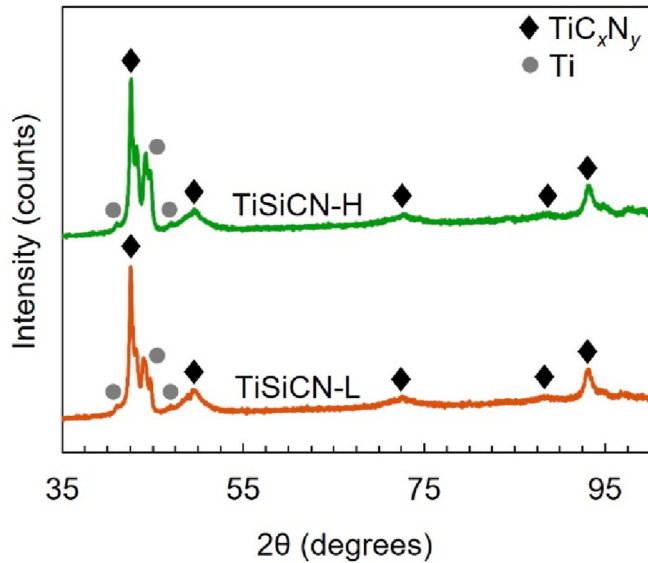


Fig. 1. TiSiCN-L (orange) and TiSiCN-H (green) coating XRD patterns. The pattern background intensities have been offset along the y-axis for visibility. (For interpretation of the references to colour in this figure legend, the reader is referred to the Web version of this article.)

during sliding wear, the elemental composition of TiSiCN coatings can be optimized by varying reactive gas flow rates during growth. With increased C-content, the coefficient of kinetic friction has been reduced

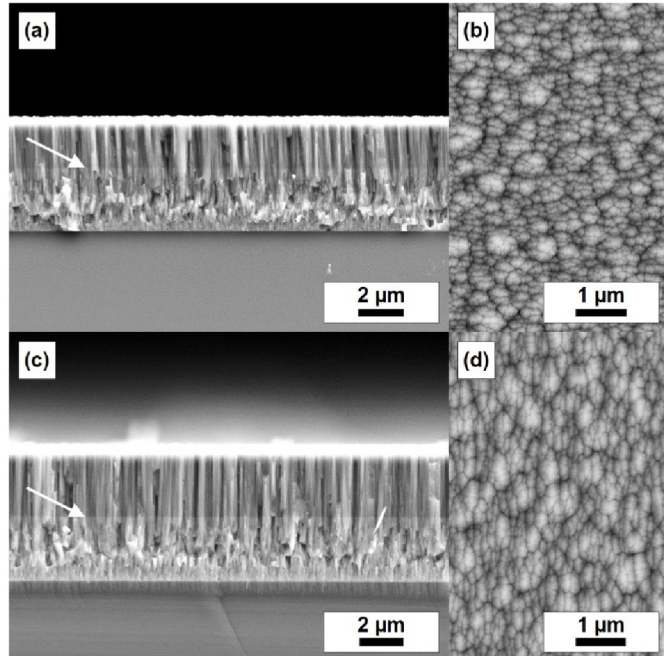


Fig. 2. Fracture cross section SEM micrographs of the TiSiCN-L (a) and TiSiCN-H (c) coatings and top-view SEM micrographs of the TiSiCN-L (b) and TiSiCN-H (d) coatings. White arrows identify the location of the interface between the interlayer and top layer for each coating.

to magnitudes on the order of 0.2 during dry sliding of TiSiCN against 304 stainless steel [15]. The tribological performance of low friction TiSiCN coatings has been evaluated using light-duty gasoline and heavy-duty diesel engine tests with TiSiCN-coated piston rings. Results demonstrated that TiSiCN piston ring coatings may be able to reduce friction losses and improve the durability of piston assemblies [15].

As friction and wear are system responses, there remain several

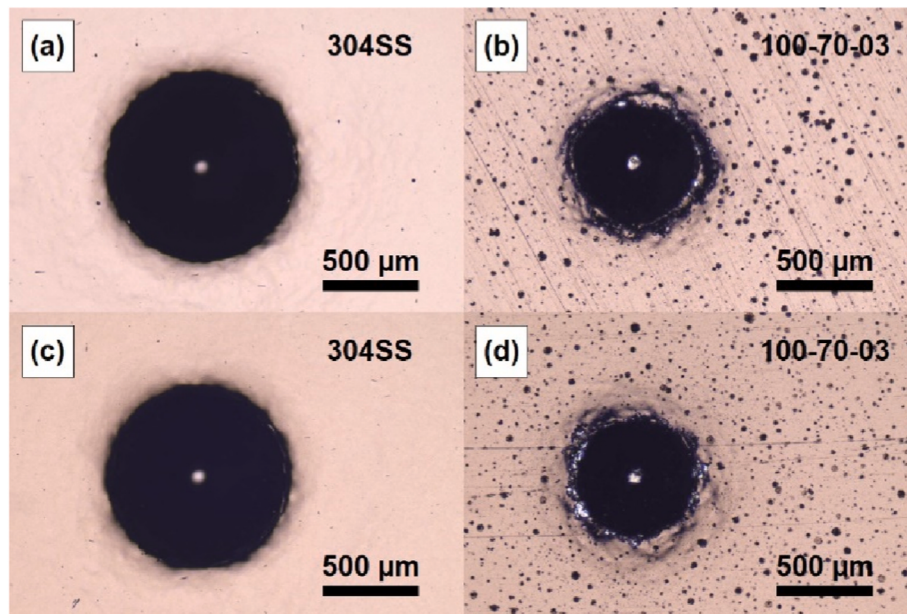


Fig. 3. Optical micrographs of Rockwell adhesion test indentations in the surfaces of 304 stainless steel (a, c) and 100-70-03 ductile iron (b, d) coated with TiSiCN-L (a, b) or TiSiCN-H (c, d).

Table 4

Hardness, apparent Young's modulus, and H/E ratios of the developmental TiSiCN coatings.

Coating	Hardness (GPa)	Apparent Young's Modulus (GPa)	H/E
TiSiCN-L	17.9 ± 3.0	217 ± 21	0.082
TiSiCN-H	16.2 ± 3.5	205 ± 28	0.079

unexplored aspects of engine component surface engineering that should be evaluated for TiSiCN coatings. While previous studies have focused only on piston ring coatings [15], the entire piston assembly (piston ring and/or cylinder liner) can be coated with TiSiCN using PVD. Therefore, it would be informative to evaluate the performance of ceramic-on-ceramic mating surfaces in addition to a tribosystem in which the chemically less-reactive coating (i.e., TiSiCN) is present on only one of the wearing surfaces. TiSiCN-TiSiCN wearing surface pairs may be mutually less abusive to each ceramic surface while

TiSiCN-metal wearing surface pairs may allow a strong chemical boundary film to be formed on the uncoated ferrous surface [12]. In this study, an evaluation of the performance of TiSiCN-metal pairs and TiSiCN-TiSiCN pairs during lubricated sliding wear was conducted. This study utilized substrates, lubricants, and test conditions that have not been investigated previously. The performance of advanced ceramic coatings in engine applications is dependent on the adhesion of the coating to the specific substrate material, the coating's chemical stability with different fuels, oils, or additives (which may have been optimized for use with ferrous materials [20]), and the tribological behaviour of the coating under varying degrees of hydrodynamic,

Table 5

Block and ring coating elemental compositions.

Coating	Ti (at.%)	Si (at.%)	C (at.%)	N (at.%)	O (at.%)
TiSiCN-L-BLOCKS	30	3	32	33	2
TiSiCN-L-RINGS	29	4	30	33	4

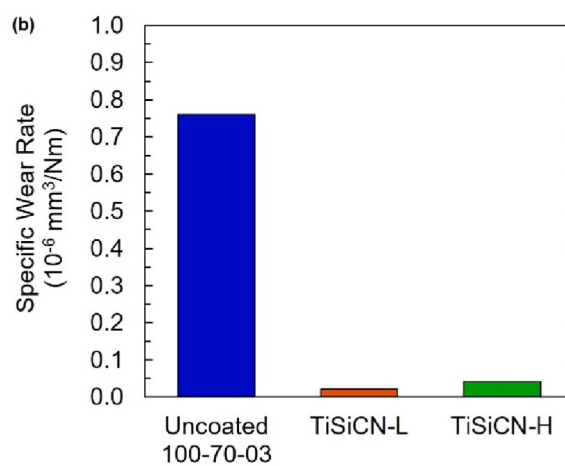
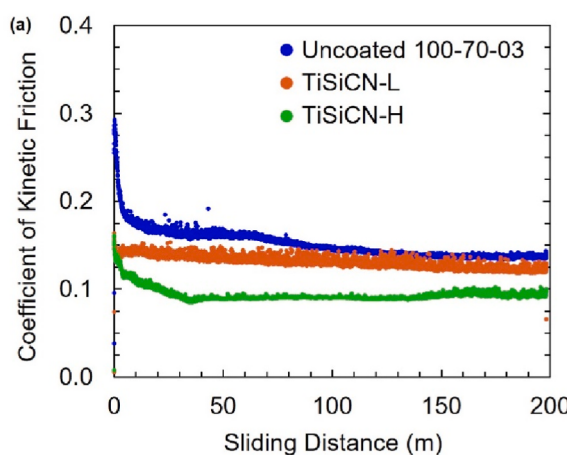


Fig. 4. Coefficient of kinetic friction during 200 m of sliding wear (a) and the resulting block specific wear rates (b). Results for the uncoated 100-70-03 blocks are plotted in blue, results for the TiSiCN-L blocks are plotted in orange, and results for the TiSiCN-H blocks are plotted in green. (For interpretation of the references to colour in this figure legend, the reader is referred to the Web version of this article.)

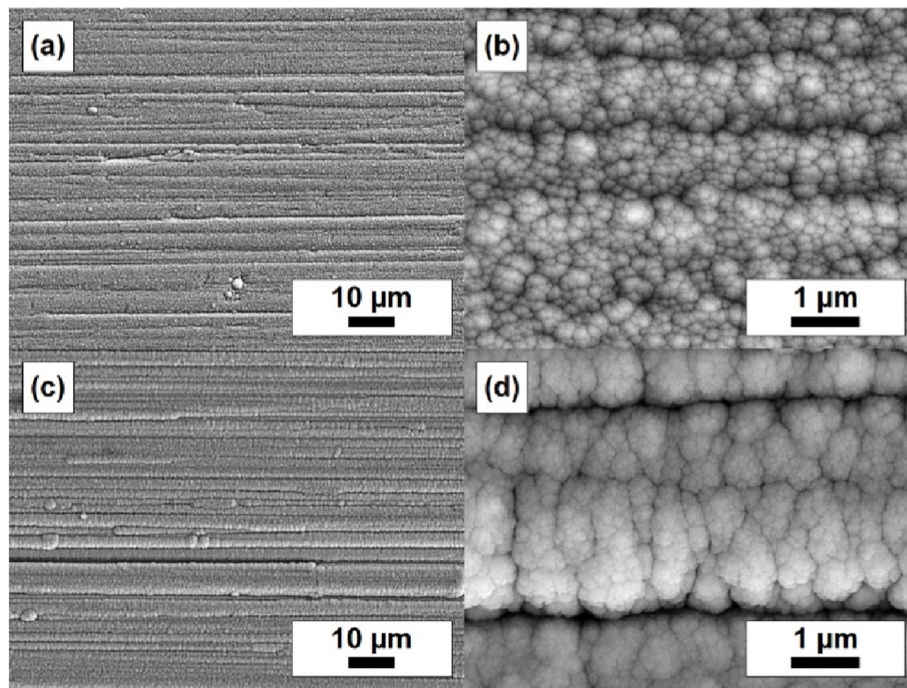


Fig. 5. Top-view SEM micrographs of the TiSiCN coating surfaces on a 100-70-03 ductile iron test block (a, b) and on a Falex S-10 test ring (c, d).

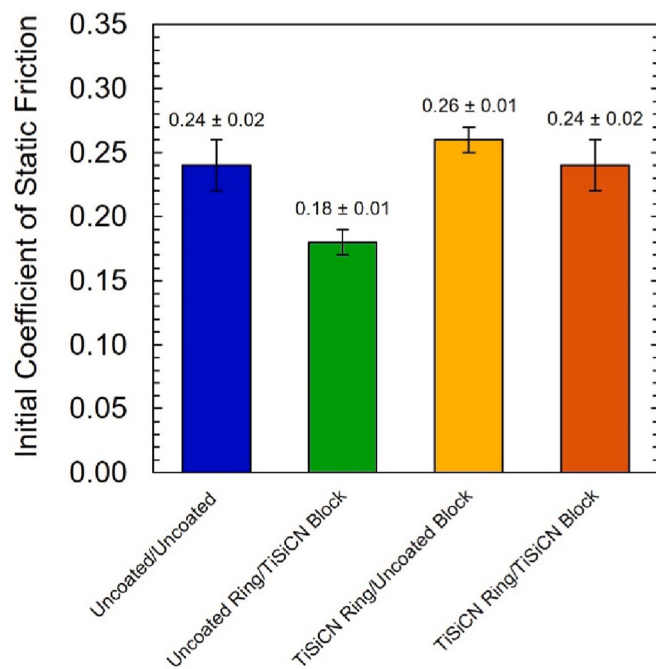


Fig. 6. Average initial coefficients of static friction for the uncoated ring/uncoated block (blue), uncoated ring/TiSiCN-coated block (green), TiSiCN-coated ring/uncoated block (yellow), and TiSiCN-coated ring/TiSiCN coated block (orange) material pairs. Error bars represent $\pm 1\sigma$. (For interpretation of the references to colour in this figure legend, the reader is referred to the Web version of this article.)

mixed, and boundary lubrication. In past research [15], TiSiCN coatings were deposited on commercially available piston rings, some of which already were coated with thermal sprayed layers, and tested in SAE 10W-30 and SAE 5W-20 oil. The present work expands on this body of knowledge by depositing TiSiCN coatings directly onto uncoated ductile

iron and evaluating the tribological performance in a SAE 15W-40 heavy-duty diesel motor oil.

2. Materials & methods

2.1. Coating deposition

Filament-assisted reactive magnetron sputtering (commonly known as plasma-enhanced magnetron sputtering [21]) was used for TiSiCN coating deposition. This advanced sputter deposition technique employs heated filaments for enhanced ionization of process gases resulting in coatings with improved adhesion and properties relative to coatings deposited by conventional DC magnetron sputtering [22] and high-power impulse magnetron sputtering [16]. The deposition system contained two rectangular magnetrons (20.32 cm \times 12.70 cm) positioned in a horizontal sputtering geometry within a 1 m³ vacuum chamber. Tungsten (W) filaments (99.95% purity, 112 cm long) were partially extended around the circumference of the deposition chamber at height levels above and below the magnetrons. A substrate holder, capable of single-fold or two-fold (i.e., planetary) rotation, was located at the center of the deposition system. Stainless steel coupons (SAE 304, annealed, 25.4 \times 25.4 \times 1.91 mm, No. 8 mirror finish), Si wafers (N-type, <100> orientation, 525 μ m thickness), and ductile iron disks (grade 100-70-03, \varnothing 25.4 mm \times 2.38 mm thick) were coated and used for destructive characterization techniques. For tribological evaluation, coatings were also applied to steel test blocks (Falex H-30, SAE O1, HRC 27–33), steel test rings (Falex S-10, SAE 4620, HRC 58–63), and ductile iron blocks (grade 100-70-03, HRC 21) with dimensions and properties conforming to ASTM G77 [23]. All substrates were cleaned with degreaser solution, acetone, and methanol prior to fixturing within the deposition chamber.

Preceding deposition, the vacuum chamber was evacuated to base pressures below 1.733 mPa (1.3×10^{-5} Torr) and then backfilled with ultra-high purity Ar (99.999%) to a working pressure of 0.333 Pa (2.5 mTorr). Substrate surfaces were etched with filament-generated Ar ions for 60 min at a DC substrate bias of -120 V and a filament discharge current and voltage of 5 A and -120 V, respectively. Two Ti targets (99.7% purity) were conditioned for 10 min after substrate ion etching,

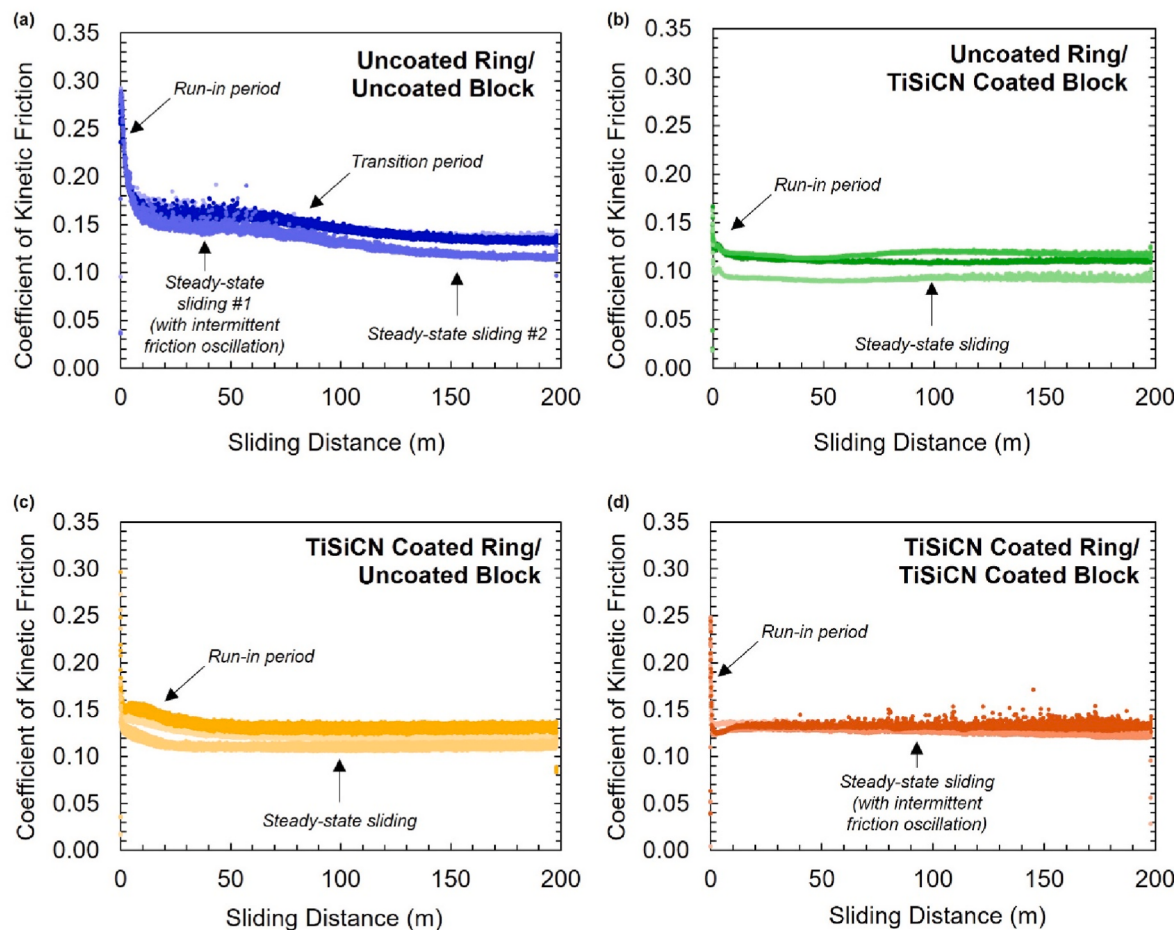


Fig. 7. Coefficient of kinetic friction versus sliding distance for the uncoated ring/uncoated block (a), uncoated ring/TiSiCN-coated block (b), TiSiCN-coated ring/uncoated block (c), and TiSiCN-coated ring/TiSiCN-coated block (d). Three test replicates were conducted for each tribosystem; results from each test are overlaid in each respective plot.

while the substrate coupons were shielded from the Ti flux. During coating deposition, continuous DC magnetron sputtering of the Ti targets was conducted in power regulation mode at 1000 W. A reactive mixture of ultra-high purity N₂ gas (99.999% purity), industrial grade acetylene (C₂H₂) gas (98% purity), and hexamethyldisilazane (HMDS) vapor (98% purity) was used to form the TiSiCN layers. HMDS is an organosilicon compound which functions as a chemical vapor precursor (i.e., as a source of Si and C) for TiSiCN synthesis [19,24]. The flow rates of N₂ and C₂H₂ were controlled by mass flow controllers while the HMDS was introduced to the deposition chamber using a conventional vapor delivery system with an external metering valve marked with vernier divisions. Interlayers between the substrates and the coating top layers were formed by gradually introducing the reactive gases while sputtering Ti. During interlayer deposition, the substrates were biased at -40 V. After the maximum flow rates were reached for the reactive gases, TiSiCN top layers were deposited at a substrate bias voltage of -60 V. Throughout deposition, the filament currents were monitored to maintain a discharge current of 5 A. Single-fold substrate rotation was used for coating deposition onto planar substrates (stainless steel coupons, Si wafers, test blocks) while two-fold substrate rotation was used for coating deposition onto the outer diameter of the test rings. After deposition, the vacuum chamber was cooled to room temperature before it was vented, and the specimens were retrieved.

Table 1 presents the conditions used for TiSiCN deposition. Initially, two TiSiCN formulations were deposited to investigate the sensitivity of coating microstructure, adhesion, mechanical properties, and oil-lubricated sliding wear performance to slight variations in elemental

composition on the order of ± 5 atomic percent (at.-%). The dry, sliding coefficient of friction of TiSiCN coatings has been reported to vary by as much as 0.15 over similar composition ranges [15]. Elemental composition was varied by increasing HMDS flow settings from 20 divisions (defined as low, "L", in Table 1) to 25 divisions (defined as high, "H", in Table 1) on the vapor delivery metering valve. In the second phase of this study, the influence of material pairing on the oil-lubricated sliding wear performance was conducted. A single TiSiCN formulation (TiSiCN-L) was deposited on the 100-70-03 ductile iron test blocks and on the Falex S-10 test rings. Tests were then conducted with the coated and uncoated wearing surfaces (blocks) and the coated and uncoated counter surfaces (rings). For these coatings, the identifications presented in Table 1 refer to the HMDS flow level ("L" for low) in addition to the type of substrate used ("BLOCKS" versus "RINGS").

2.2. Coating characterization & testing

Coating elemental compositions were measured using energy dispersive X-ray spectroscopy (EDS). X-ray spectra were collected with an Oxford Instruments 80 mm² silicon drift detector in a ZEISS Supra 40VP field-emission scanning electron microscope (SEM). X-ray diffraction (XRD) patterns were collected from the coated Si wafer specimens using a Malvern Panalytical Empyrean diffractometer with Co radiation ($\lambda_{K\alpha} = 0.179$ nm). The XRD scans were conducted using the Bragg-Brentano 0:0 geometry. SEM was used to characterize the morphologies of the coating surfaces and fracture cross sections. The practical adhesion of the TiSiCN coatings to stainless steel and ductile iron

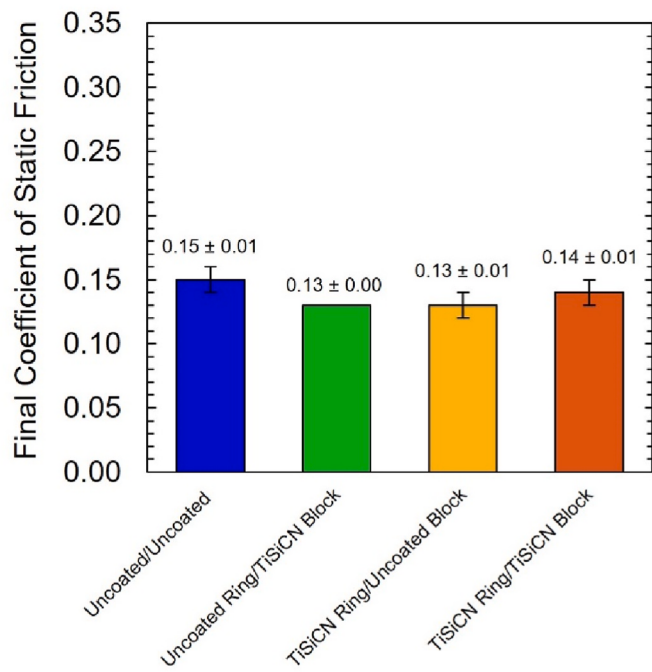


Fig. 8. Average final coefficients of static friction for the uncoated ring/uncoated block (blue), uncoated ring/TiSiCN-coated block (green), TiSiCN-coated ring/uncoated block (yellow), and TiSiCN-coated ring/TiSiCN coated block (orange) material pairs. Error bars represent $\pm 1\sigma$. (For interpretation of the references to colour in this figure legend, the reader is referred to the Web version of this article.)

was qualitatively assessed by Rockwell indentation tests using a 120° spherconical diamond indenter and a 150 kg load [25]. The residual indentations were analyzed using a ZEISS Axio Vert.A1 optical microscope. An MTS Nanoindenter XP with a diamond Berkovich indenter was used to measure coating hardness and apparent (i.e., substrate-affected) Young's modulus. A fused silica reference sample was used to complete tip area function and instrument frame stiffness calibrations prior to testing. Thirty indentations were made into the TiSiCN coatings at a peak load of 25 mN. Analysis was conducted using the Oliver-Pharr

technique [26] while assuming a Poisson's ratio of 0.20 for the coating materials.

The tribological performance of the TiSiCN coatings was evaluated using a block-on-ring tribometer in which test blocks were loaded against rotating test rings while the friction force required to keep the block in place was continuously measured [23]. The block-on-ring test plan is outlined in Table 2. The performance of the Falex H-30 blocks (27–33 HRC) coated with TiSiCN-L and TiSiCN-H was compared to that of an uncoated ductile iron block to establish the feasibility of improving grade 100-70-03 ductile iron performance via the application of a TiSiCN coating. Subsequent tests were conducted among various combinations of TiSiCN-coated Falex S-10 rings (TiSiCN-L-RINGS), TiSiCN-coated ductile iron blocks (TiSiCN-L-BLOCKS), uncoated Falex S-10 steel rings, and uncoated ductile iron blocks. Three replicates of each test condition were performed. Prior to testing, all blocks and rings were ultrasonically cleaned using a degreaser solution and then rinsed with methanol. Tests were conducted in John Deere Plus-50 II (SAE 15W-40) engine oil, suitable for use in heavy-duty off-road equipment, on-road trucks, marine engines, and natural gas engines. The oil was heated to 127 °C during testing. The normal loads, sliding speeds, and sliding distances were held constant for all tests. Coefficients of static and kinetic friction were recorded for each test. After block-on-ring testing, the worn test blocks were characterized using SEM and a Keyence VK-X250 profile-measuring laser microscope. Block wear scar volumes (i.e., block volume losses) were calculated from the wear scar widths using the method of ASTM G77 [23]. The specific wear rates, $K = V/(w \cdot s)$, were subsequently calculated from the block wear scar volumes (V), the normal load ($w = 222$ N), and the distance slid ($s = 200$ m).

3. Results & discussion

3.1. Variation of TiSiCN composition

TiSiCN-L and TiSiCN-H coatings, with low and high Si contents, were obtained by manipulating the availability of the organosilicon precursor vapor during coating growth (see Table 1). The elemental compositions of these two coating formulations, as measured by EDS, are shown in Table 3. The Si and C contents are greater in TiSiCN-H by 2 at.% and 3 at.%, respectively. The measured O content is low in both coating formulations. In comparison with previously reported TiSiCN coatings

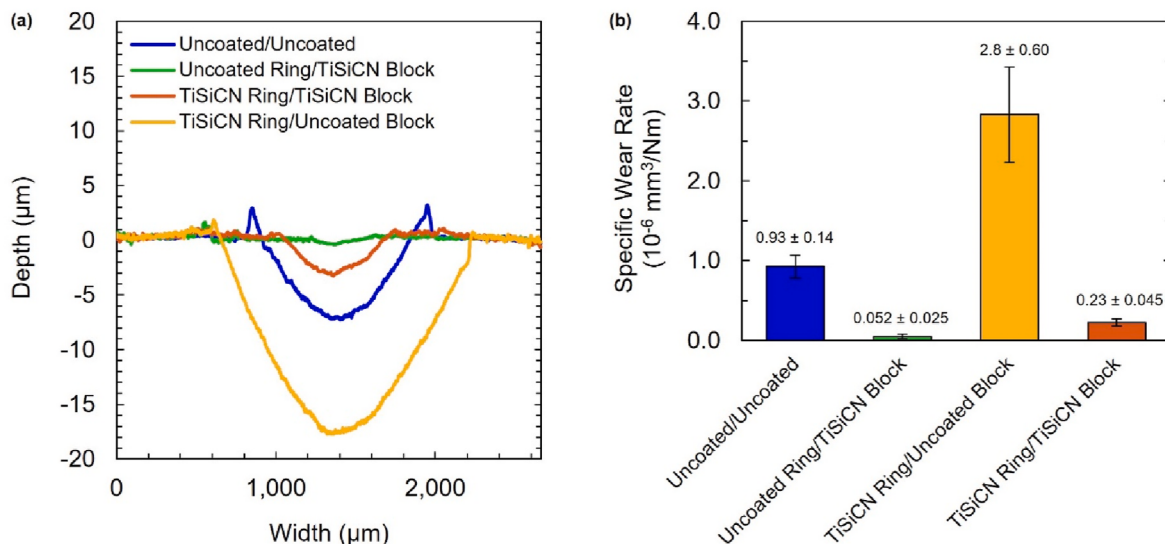


Fig. 9. Representative wear scar profiles (a) and the average specific wear rates calculated from block wear scar widths (b) for the uncoated ring/uncoated block (blue), uncoated ring/TiSiCN-coated block (green), TiSiCN-coated ring/uncoated block (yellow), and TiSiCN-coated ring/TiSiCN coated block (orange) material pairs. Error bars represent $\pm 1\sigma$. (For interpretation of the references to colour in this figure legend, the reader is referred to the Web version of this article.)

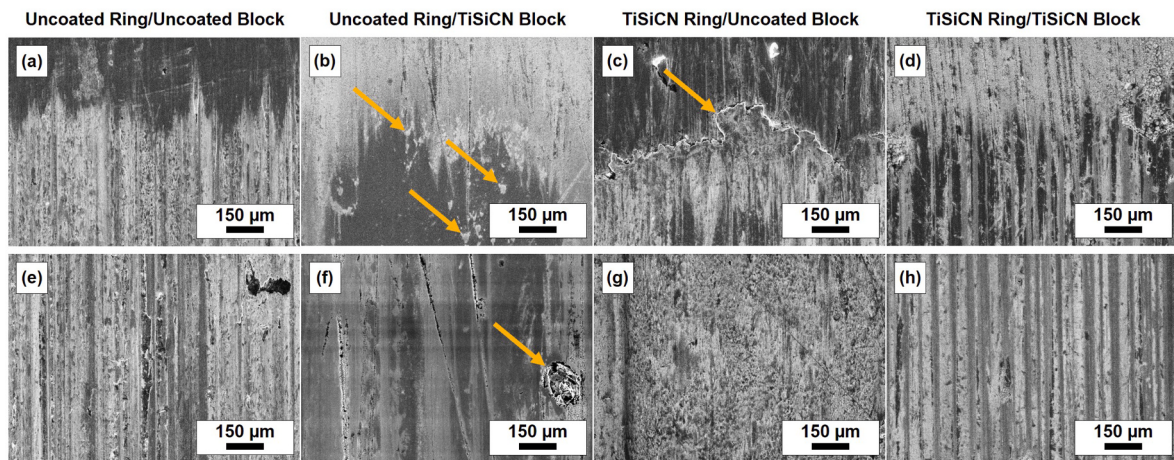


Fig. 10. SEM micrographs of block surfaces at the edge of the wear scar (a, b, c, d) and in the center of the wear scar (e, f, g, h) for the uncoated ring/uncoated block (a, e), uncoated ring/TiSiCN block (b, f), TiSiCN ring/uncoated block (c, g), and TiSiCN ring/TiSiCN block (d, h) material pairs. Arrows identify patches of debris (b), accumulated edge debris (c), and localized severe coating damage (f).

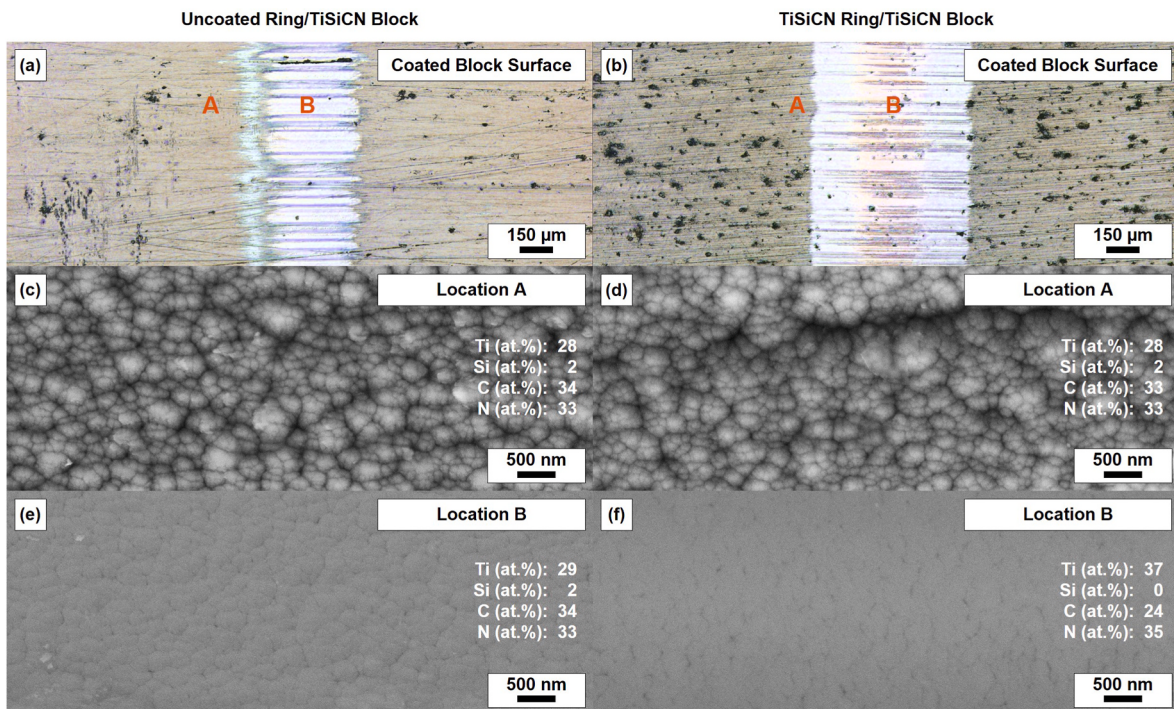


Fig. 11. Optical micrographs (a, b) and SEM micrographs (c, d, e, f) of the wear scar regions from the uncoated ring/TiSiCN-coated block (a, c, e) and TiSiCN-coated ring/TiSiCN-coated block (b, d, f) material pairs. SEM micrographs were acquired from unworn surface regions (Location A) and regions in the center of the wear scars (Location B). EDS results are provided with the SEM micrographs.

optimized for piston ring applications, these coatings have a lower Ti content (<30 at.% versus >40 at.%) and a greater C content (>30 at.% versus <30 at.%) [15].

The XRD patterns obtained from the TiSiCN-L and TiSiCN-H coatings are shown in Fig. 1. The primary diffraction peaks observed in both patterns are associated with a cubic (NaCl-type) TiC_xN_y phase, consistent with the phases identified in other TiSiCN coatings deposited under similar growth conditions [15]. Peaks associated with α -phase Ti can also be detected in the diffraction patterns and originate from the coating layers that were grown prior to the introduction of reactive gases. Overall, significant differences between the TiSiCN-L and TiSiCN-H diffraction patterns are not seen which indicates that the phase content of the coatings is not sensitive to slight changes in Si and C

content.

SEM micrographs of the TiSiCN coatings are presented in Fig. 2. Cross-sectional micrographs, obtained from fractured Si wafer specimens, are shown in Fig. 2(a) and (c) for TiSiCN-L and TiSiCN-H, respectively. The growth structures of both coatings are characterized as dense and columnar. The location of the interface between the interlayers, formed during the gradual introduction of reactive gases, and the top layers, formed after final reactive gas flow rates were held constant, is evidenced by a change in contrast in the electron micrographs (identified by the white arrows in Fig. 2). The total thickness of TiSiCN-L is 5.2 μm and the total thickness of TiSiCN-H is 6.2 μm , indicating that the overall growth rate for both coating formulations was about 1.8 $\mu\text{m}/\text{h}$ (per Table 1, deposition durations were varied between

the two coatings during process development). Top-view micrographs of the TiSiCN-L and TiSiCN-H surfaces on the mirror-finish 304 stainless steel coupons are shown in Fig. 2(b) and (d), respectively. The surfaces of both coatings are dense and have nodular morphologies characteristic of coatings deposited by filament-assisted DC magnetron sputtering [16]. In summary, the growth structures and surface morphologies of the TiSiCN coating formulations were not affected by the variation in Si and C content.

Optical micrographs of the Rockwell adhesion test indentations are presented in Fig. 3. The indentation tests were performed on annealed 304 stainless steel (HRC <20) and hardened 100-70-03 ductile iron (HRC 55) substrates. The difference in residual indentation size results from the hardness difference between the two substrate materials, with the 100-73-03 ductile iron having higher hardness and therefore smaller diameter indentations. The spheroidal graphite nodules in the ductile iron substrates manifest as dark spots on the coating surface. TiSiCN-L and TiSiCN-H have excellent adhesion to both stainless steel and ductile iron as there are only minimal signs of coating delamination around the periphery of the indentation shown in Fig. 3(d). The excellent adhesion results from the use of the heated filaments to ion etch the substrate surfaces and to achieve favourable growth conditions.

The mechanical properties of the TiSiCN coatings, as measured by nanoindentation, are presented in Table 4. The high Si and C content of TiSiCN-H resulted in comparatively lower hardness and apparent Young's modulus. However, the H/E ratios, which can serve as wear resistance indicators [27], are comparable for both TiSiCN-L and TiSiCN-H. The hardness of TiSiCN coatings optimized for piston ring applications has been reported in the range of 14–15 GPa, while the Young's modulus was reported around 175 GPa [15]. As observed in Table 4, both hardness and apparent Young's modulus were higher for the coatings prepared in this study.

The results from the preliminary block-on-ring tests (Tests #1–3, Table 2) are presented in Fig. 4. The coefficients of kinetic friction (μ_k) that were measured continuously during testing are plotted as a function of sliding distance in Fig. 4(a) while the resulting block specific wear rates are presented in Fig. 4(b). For both coating formulations, μ_k stabilizes after 50 m of sliding while the kinetic friction behaviour of the uncoated ductile iron block does not stabilize until 100 m of sliding distance. The TiSiCN-H coating exhibited the lowest coefficient of kinetic friction with an average steady-state value of 0.091 ± 0.002 . TiSiCN-L and the uncoated ductile iron samples exhibited average coefficients of kinetic friction of 0.128 ± 0.005 and 0.139 ± 0.003 , respectively. These μ_k magnitudes are consistent with expectations for boundary lubrication conditions ($\mu_k \geq 0.1$) [3,12]. Fig. 4(b) illustrates that the test block wear resistance improved when the surface was coated with TiSiCN, regardless of the coating composition. A slight decrease in specific wear rate, however, was measured for the TiSiCN-L coating ($0.0214 \cdot 10^{-6} \text{ mm}^3/\text{Nm}$) relative to the TiSiCN-H coating ($0.0408 \cdot 10^{-6} \text{ mm}^3/\text{Nm}$). While test replicates would have been required to make conclusive comparisons [23], the preliminary tribological evaluation demonstrated the feasibility of using TiSiCN coatings to improve the wear resistance of grade 100-70-03 ductile iron in a tribological environment resembling heavy-duty diesel engine operation. Additionally, the tests indicated that, at worst, the TiSiCN-coated surfaces would exhibit comparable friction behaviour to uncoated ductile iron.

3.2. Variation of mating material

TiSiCN-L-BLOCKS and TiSiCN-L-RINGS were used to evaluate the performance of the following material pairs: (i) uncoated steel rings sliding against uncoated ductile iron blocks ("uncoated ring/uncoated block"), (ii) uncoated rings sliding against TiSiCN-coated blocks ("uncoated ring/TiSiCN block"), (iii) TiSiCN-coated rings sliding against uncoated ductile iron blocks ("TiSiCN ring/uncoated block"), (iv) TiSiCN-coated rings sliding against TiSiCN-coated blocks ("TiSiCN ring/

TiSiCN block"). The elemental compositions of the TiSiCN-L-BLOCKS and TiSiCN-L-RINGS coatings are presented in Table 5. Two-fold planetary rotation was utilized to coat the external surface of the rings while the planar block surfaces were coated using single-fold rotation. This resulted in greater incorporation of Si and O from the reactive vapor environment and a decreased concentration of Ti in TiSiCN-L-RINGS due to reduced residence time in regions of the chamber with high fluxes of sputtered species [28]. The block coating composition also differs slightly from the composition of TiSiCN-L on 304 stainless steel coupons (Table 3). This is attributed to a change in source-to-substrate distance due to the greater thickness of the blocks (10.16 mm versus 1.91 mm).

Fig. 5 displays SEM micrographs of the surfaces of a representative block coating (a, b) and a representative ring coating (c, d). The machined surface finishes of the blocks and rings are still visible after coating deposition, which suggests that the application of thin coatings to honed cylinder liners may not necessarily require post-deposition finishing. The morphology of the coatings is again characterized as nodular; however, the coating substructure size does differ between the block specimens deposited using single-fold rotation and the ring specimens deposited using two-fold planetary rotation.

Immediately prior to the block-on-ring sliding wear tests, the initial coefficient of static friction (μ_s) was measured for each tribosystem using the block-on-ring tribometer. Three successive μ_s measurements were made with the oil-wetted contacting surfaces; the average results are shown in Fig. 6. The lowest initial coefficient of static friction of 0.18 ± 0.10 was exhibited by the uncoated ring/TiSiCN-coated block material pair.

The coefficient of kinetic friction was continuously measured during the sliding wear tests for each material pair. Results from these sliding wear tests are shown in Fig. 7. Three test replicates were run for each of the four different tribosystems. Results for the uncoated ring/uncoated block, uncoated ring/TiSiCN block, TiSiCN ring/uncoated block, and TiSiCN ring/TiSiCN block are shown in Fig. 7(a), 7(b), 7(c), and 7(d), respectively.

The friction behaviour of the uncoated ring/uncoated block material pair, shown in Fig. 7(a), is characterized by a run-in period followed by an initial steady-state sliding period between 10 m and 75 m, which transitioned gradually into a second steady-state sliding period that continued throughout the remainder of the test. The first steady-state state sliding period exhibited intermittent friction oscillation, possibly resulting from stick-slip between the two iron-rich surfaces given that the initial coefficient of static friction of the tribosystem was 0.24 ± 0.02 and the average coefficient of kinetic friction during this sliding period was 0.16 ± 0.01 (i.e., $\mu_s > \mu_k$). After the gradual transition period (i.e., after 100 m of sliding), the overall average steady-state μ_k calculated from all three test replicates was 0.13 ± 0.01 .

The friction behaviour of the uncoated ring/TiSiCN block material pair, shown in Fig. 7(b), is characterized by a brief run-in period followed by a steady-state sliding period that continued for the remaining duration of the test. Unlike the first steady-state sliding period for the uncoated ring/uncoated block material pair, significant oscillation in the friction force was not observed. After 50 m of sliding, the overall average steady-state μ_k was 0.11 ± 0.01 .

The friction behaviour of the TiSiCN ring/uncoated block material pair, shown in Fig. 7(c), was similar to the behaviour of the uncoated ring/TiSiCN block material pair (Fig. 7(b)). After 50 m of sliding, the overall average steady-state μ_k was 0.12 ± 0.01 . From inspection of Fig. 7(b) and (c) it can be observed that μ_k variability within individual tests was greater for the TiSiCN ring/uncoated block material pair than for the uncoated ring/TiSiCN block material pair.

The TiSiCN-coated ring/TiSiCN-coated block material pair demonstrated very consistent behaviour among replicate tests, as seen in Fig. 7(d). After a brief run-in period, the steady-state μ_k data exhibited intermittent oscillation, especially as the test progressed. After 50 m of sliding, the overall average steady-state μ_k was 0.129 ± 0.004 .

The average final coefficient of static friction for each material pair is

presented in Fig. 8. The final μ_s is comparable for all material pairs and the averages all fell within the range of 0.13–0.15, which is lower than the range of initial coefficients of static friction (Fig. 6).

Results from the analysis of the wearing surfaces are presented in Fig. 9. In Fig. 9(a), representative wear scar profiles from the blocks of each material pair are plotted and in Fig. 9(b) the average block specific wear rates are displayed. From inspection of these results, it can be concluded that the wear resistance of the ductile iron blocks improved when coated with TiSiCN. It can also be observed that when the ring-component of the material pair is coated with TiSiCN, the wear of the counterface block increases relative to the corresponding material pair in which the ring is uncoated. These results highlight the importance of considering cylinder liner coatings given the current interest in coating piston rings with hard coatings such as CrN [29,30], diamond-like-carbon [31], and TiSiCN [15]. Evaluation of ring wear resistance was not possible since all rings tested in this study experienced negligible mass losses.

SEM micrographs of the representative block wear scars are provided in Fig. 10. The top row of micrographs (a, b, c, d) were acquired from regions near the edge of the wear scars while the bottom row of micrographs (e, f, g, h) were acquired from regions located at the center of the wear scars. Ploughed grooves oriented parallel to the sliding direction are observed for the uncoated block that wore against an uncoated ring (Fig. 10.a, Fig. 10.e). Evidence of smeared material is also visible in Fig. 10.e. The damage to the TiSiCN block that wore against an uncoated ring (Fig. 10.b, Fig. 10.f) is relatively less severe. Significant ploughed grooves are not observed, and the coated block surface appears polished. Evidence of localized patches of transfer layer material can be seen in Fig. 10.b and localized damage to the coating, which possibly corresponds to the location of a graphite nodule, can be seen in Fig. 10.f. The wear of the uncoated ductile iron block paired with the TiSiCN-coated ring (Fig. 10.c, Fig. 10.g) was severe. Edge debris accumulation is evident in Fig. 10.c and the center of the wear scar is covered in smeared material (Fig. 10.g). Similar to the uncoated block, the wear scar on the TiSiCN block that wore against a TiSiCN ring (Fig. 10.d, Fig. 10.h) is characterized by the presence of ploughed grooves oriented parallel to the sliding direction. Apart from the localized damage observed in Fig. 10.f, neither of the coated block surfaces exhibit extensive signs of coating failure such as spallation or cracking.

Additional analysis of the TiSiCN-coated blocks was conducted using optical microscopy, SEM, and EDS. Fig. 11 displays optical micrographs of the wear scars (a, b), SEM micrographs from the unworn areas of the blocks (c, d), and SEM micrographs from the center of the wear scars (e, f) for the uncoated ring/TiSiCN-coated block (a, c, e) and TiSiCN-coated ring/TiSiCN-coated block (b, d, f) material pairs. EDS results, shown in Fig. 11, reveal that the ductile iron base has not been exposed by wear for either material couple. For the uncoated ring/TiSiCN-coated block material pair (Fig. 11.e), the presence of Si in the wear scar EDS spectra indicates that the TiSiCN top layer was not worn through completely. However, the absence of Si in the wear scar EDS spectra obtained from the TiSiCN ring/TiSiCN-coated block material pair (Fig. 11.f) indicates that the exposed surface corresponds to the TiCN interlayer and therefore the top layer was removed by wear. From inspection of the SEM micrographs, nanoporosity at coating column boundaries is visible on both wearing surfaces. Additionally, both wear scar surfaces appear polished and smooth without signs of accumulated or reattached wear debris.

4. Conclusions

In this work, two compositions of TiSiCN coatings were deposited onto 100-70-03 ductile iron. Both formulations had nodular morphologies, exhibited similar H/E ratios (~0.8), and had excellent adhesion to ductile iron. The TiSiCN coatings also performed better than uncoated 100-70-03 ductile iron during preliminary sliding wear tests. Subsequently, a TiSiCN coating with 3–4 at.% Si was selected for further

tribological evaluation of various mating material combinations and was deposited on test blocks and rings. Intermittent oscillation in the friction force was observed for self-mated TiSiCN, particularly at greater sliding distances. Tribosystems in which only one wearing surface was coated with TiSiCN exhibited coefficients of kinetic friction that were more stable over the duration of the sliding wear tests relative to the behaviour of uncoated 100-70-03 ductile iron. Thus, the physical and chemical interactions of the oil with the TiSiCN coatings did not adversely affect the friction behaviour and improved run-in performance was obtained. The wear resistance of the block surfaces was improved when coated with TiSiCN (>24% reduction in block specific wear rate relative to uncoated ductile iron) but the presence of TiSiCN on the ring counter surface resulted in increased block wear (>300% increase in uncoated block specific wear rate relative to uncoated ring pair). The TiSiCN wear mechanism did not involve extensive coating fracture nor delamination from the ductile iron. The results of this study demonstrate the improved tribological performance of TiSiCN-coated ductile iron relative to uncoated ductile iron during oil-lubricated sliding wear and highlight the importance of considering advanced coatings for cylinder bores in heavy-duty internal combustion engines.

CRediT author statement

Forest C. Thompson: Conceptualization, Methodology, Investigation, Visualization, Writing – Original Draft **Frank M. Kustas:** Conceptualization, Resources, Writing – Review & Editing **Grant A. Crawford:** Supervision, Conceptualization, Project Administration, Funding Acquisition, Writing – Review & Editing.

Declaration of competing interest

The authors declare that they have no known competing financial interests or personal relationships that could have appeared to influence the work reported in this paper.

Data availability

Data will be made available on request.

Acknowledgements

This work was supported in part by John Deere. Any opinions, findings, and conclusions or recommendations expressed in this material are those of the author(s) and do not necessarily reflect the views of John Deere. The authors gratefully acknowledge Mr. James Tomich (Arbegast Materials Processing and Joining Laboratory, South Dakota School of Mines and Technology) and Mr. Kelsey Fitzgerald (NanoCoatings, Inc.) for their assistance in sample preparation and testing.

References

- [1] Ductile iron, in: J.R. Davis (Ed.), Metals Handbook: Desk Edition, ASM International, Materials Park (OH), 1998, pp. 314–320.
- [2] Wear of cast irons, in: D.M. Stefanescu (Ed.), Cast Iron Science and Technology, ASM Handbook, 1A, ASM International, Materials Park (OH), 2017, pp. 489–501.
- [3] V.W. Wong, S.C. Tung, Friction, lubrication, and wear of internal combustion engine parts, in: G.E. Totten (Ed.), Friction, Lubrication, and Wear Technology, ASM Handbook, 18, ASM International, Material Park (OH), 2017, pp. 899–915.
- [4] P.H. Mayrhofer, C. Mitterer, L. Hultman, et al., Microstructural design of hard coatings, Prog. Mater. Sci. 51 (8) (2006) 1032–1114, <https://doi.org/10.1016/j.pmatsci.2006.02.002>.
- [5] J. Musil, Hard nanocomposite coatings: thermal stability, oxidation resistance and toughness, Surf. Coat. Technol. 207 (2012) 50–65, <https://doi.org/10.1016/j.surfcoat.2012.05.073>.
- [6] H. Kindlund, D.G. Sangiovanni, I. Petrov, et al., A review of the intrinsic ductility and toughness of hard transition-metal nitride alloy thin films, Thin Solid Films 688 (2019), 137479, <https://doi.org/10.1016/j.tsf.2019.137479>.
- [7] H. Kindlund, D.G. Sangiovanni, L. Martínez-de-Olcoz, et al., Toughness enhancement in hard ceramic thin films by alloy design, Apl. Mater. 1 (2013), 042104, <https://doi.org/10.1063/1.4822440>.

- [8] A.A. Voevodin, C. Muratore, S.M. Aouadi, Hard coatings with high temperature adaptive lubrication and contact thermal management: Review, *Surf. Coat. Technol.* 257 (2014) 247–265, <https://doi.org/10.1016/j.surfcoat.2014.04.046>.
- [9] R. Wei, inventor; Southwest Research Institute, assignee, Method for Magnetron Sputter Deposition, 2006 Apr 13. United States patent application publication US2006/0076231 A1.
- [10] M. Panjan, Influence of substrate rotation and target arrangement on the periodicity and uniformity of layered coatings, *Surf. Coat. Technol.* 235 (2013) 32–44, <https://doi.org/10.1016/j.surfcoat.2013.06.126>.
- [11] P. Pawlus, R. Reizer, Functional importance of honed cylinder liner surface texture: a review, *Tribol. Int.* 167 (2022), 107409, <https://doi.org/10.1016/j.triboint.2021.107409>.
- [12] B. Bhushan, *Introduction to Tribology*, Wiley, New York (NY), 2002.
- [13] P. Panjan, A. Drnovšek, M. Čekada, et al., Contamination of substrate-coating interface caused by ion etching, *Coatings* 12 (6) (2022) 846, <https://doi.org/10.3390/coatings12060846>.
- [14] G. Abadias, E. Chason, J. Keckes, et al., Review article: stress in thin films and coatings: current status, challenges, and prospects, *J. Vac. Sci. Technol., A* 36 (2018), 020801, <https://doi.org/10.1116/1.5011790>.
- [15] J. Lin, R. Wei, D.C. Bitsis, et al., Development and evaluation of low friction TiSiCN nanocomposite coatings for piston ring applications, *Surf. Coat. Technol.* 298 (2016) 121–131, <https://doi.org/10.1016/j.surfcoat.2016.04.061>.
- [16] J. Lin, R. Wei, A comparative study of thick TiSiCN nanocomposite coatings deposited by dcMS and HiPIMS with and without PEIMS assistance, *Surf. Coat. Technol.* 338 (2018) 84–95, <https://doi.org/10.1016/j.surfcoat.2018.01.082>.
- [17] H.M. Lin, J.G. Duh, R. Wei, et al., The effect of microstructure and composition on mechanical properties in thick-layered nanocomposite Ti–Si–C–N coatings, *Surf. Coat. Technol.* 205 (5) (2010) 1460–1464, <https://doi.org/10.1016/j.surfcoat.2010.07.070>.
- [18] R. Wei, E. Langa, C. Rincon, et al., Deposition of thick nitrides and carbonitrides for sand erosion protection, *Surf. Coat. Technol.* 201 (7) (2006) 4453–4459, <https://doi.org/10.1016/j.surfcoat.2006.08.091>.
- [19] R. Wei, C. Rincon, E. Langa, et al., Microstructure and tribological performance of nanocomposite Ti–Si–C–N coatings deposited using hexamethyldisilazane precursor, *J. Vac. Sci. Technol., A* 28 (2010) 1126–1132, <https://doi.org/10.1116/1.3463709>.
- [20] S.C. Tung, V.W. Wong, Engine lubricants overview and development trends, in: G. E. Totten (Ed.), *Friction, Lubrication, and Wear Technology*, ASM Handbook, 18, ASM International, Material Park (OH), 2017, pp. 150–161.
- [21] J. Matossian, R. Wei, J. Vajo, et al., Plasma-enhanced, magnetron-sputtered deposition (PMD) of materials, *Surf. Coat. Technol.* 108–109 (1998) 496–506, [https://doi.org/10.1016/S0257-8972\(98\)00632-X](https://doi.org/10.1016/S0257-8972(98)00632-X).
- [22] A.M.A. El-Rahman, R. Wei, A comparative study of conventional magnetron sputter deposited and plasma enhanced magnetron sputter deposited Ti–Si–C–N nanocomposite coatings, *Surf. Coat. Technol.* 241 (2014) 74–79, <https://doi.org/10.1016/j.surfcoat.2013.08.049>.
- [23] ASTM G77-17, *Standard Test Method for Ranking Resistance of Materials to Sliding Wear Using Block-On-Ring Wear Test*, ASTM International, West Conshohocken (PA), 2017.
- [24] E. Ermakova, M. Kosinova, Organosilicon compounds as single-source precursors for SiCN films production, *J. Organomet. Chem.* 958 (2022), 122183, <https://doi.org/10.1016/j.jorgchem.2021.122183>.
- [25] N. Vidakis, A. Antoniadis, N. Bilalis, The VDI 3198 indentation test evaluation of a reliable qualitative control for layered compounds, *J. Mater. Process. Technol.* 143–144 (2003) 481–485, [https://doi.org/10.1016/S0924-0136\(03\)00300-5](https://doi.org/10.1016/S0924-0136(03)00300-5).
- [26] W.C. Oliver, G.M. Pharr, An improved technique for determining hardness and elastic modulus using load and displacement sensing indentation experiments, *J. Mater. Res.* 7 (1992) 1564–1583, <https://doi.org/10.1557/JMR.1992.1564>.
- [27] A. Leyland, A. Matthews, On the significance of the H/E ratio in wear control: a nanocomposite coating approach to optimised tribological behaviour, *Wear* 246 (1–2) (2000) 1–11, [https://doi.org/10.1016/S0043-1648\(00\)00488-9](https://doi.org/10.1016/S0043-1648(00)00488-9).
- [28] M. Hans, M. Baben, Y.T. Chen, et al., Substrate rotation-induced chemical modulation in Ti-Al-O-N coatings synthesized by cathodic arc in an industrial deposition plant, *Surf. Coat. Technol.* 305 (2016) 249–253, <https://doi.org/10.1016/j.surfcoat.2016.08.046>.
- [29] N. Iijima, Y. Shima, M. Hasei, Development of piston ring surface treatment on next-generation engines, *SAE Tech. Pap.* 12 (2021), <https://doi.org/10.4271/2021-01-0648>.
- [30] S. Wan, H. Wang, Y. Xia, et al., Investigating the corrosion-fatigue wear on CrN coated piston rings from laboratory wear tests and field trial studies, *Wear* 432–433 (2019), 202940, <https://doi.org/10.1016/j.wear.2019.202940>.
- [31] A. Vahidi, D. Fonseca, J. Oliveira, et al., Advanced tribological characterization of DLC coatings produced by Ne-HiPIMS for the application on the piston rings of internal combustion engines, *Appl. Sci.* 11 (2021), 10498, <https://doi.org/10.3390/app112110498>.